Study of Residual Strain in Large Area AlGaN Growth and Characterization Support

Subcontract to support EMCORE's effort on
DARPA's BAA number: 01-35
Wide Bandgap Semiconductor Technology Initiative

Technical point of contact
Ian Ferguson, Professor
School of Electrical and Computer Engineering
Georgia Institute of Technology
Atlanta, Georgia 30332-0250 U.S.A.
PHONE: 404-385-2885
EMAIL: ianf@ece.gatech.edu

1. Introduction

A large difference exists in the coefficient of thermal expansion (CTE) between the III-Nitride epitaxial layer and the substrate. This thermal mismatch leads to the generation of defects in the GaN and cracking when the hetero-epitaxial layer and the substrate are cooled from the growth temperature to room temperature after deposition. This is an important issue that needs to be addressed for the ability to produce large area III-Nitride growth on non-native substrates such as sapphire. When the strain is not relieved through cracking a significant bowing can be also observed. Additional characterization support will also be provided including high resolution X-ray diffraction, AFM, SIMS and other techniques available at GaTech. The objective is to better understand the fundamental properties of GaN FET structures and to develop evaluation methods for the optimization of these materials that relate to the operational characteristics of the device.

A detailed study of GaN and AlGaN has been completed as basis for understanding the X-ray characterization of GaN FETs. The threading dislocation densities in GaN and AlGaN epitaxial layers have been evaluated using two different X-ray analysis techniques: a Williamson-Hall (WH) plot and reciprocal space mapping (RSM). GaN and AlGaN have crystalline growth composed of columnar structures that can be estimated by coherence length and angular misorientation measured by X-ray. A WH plot can provide information about coherence length and tilt angle from a linear fit to the linewidth of the triple axis rocking curve (000*l*) symmetric reflections. RSM is typically used to obtain this data, but it is more involved in technique. The two dominant components of threading dislocation densities (screw and edge types) in the GaN and AlGaN epitaxial layers were found to be similar by both techniques. The threading dislocation density correlates to the size of the columnar structure as determined by coherence length, tilt angle, and twist angle. The effect of Al composition in AlGaN alloys on these dislocation densities was investigated and found to depend strongly on the type of nucleation layer, GaN or AlN.

Fabrication of HEMTs depends critically upon the material deposited which , in turn, depends crucially on the substrates involved. GaN is usually deposited on sapphire or silicon carbide, both of which provide high temperature processing ability with reasonable lattice matching and thermal expansion coefficients. Nevertheless, issues of the material quality dependence on substrates remain and are investigated in the second half of this report. When

depositing AlGaN layers on non-native substrates, the residual strain can be determined by analysis of the XRD of the symmetric and asymmetric peaks. Furthermore, even after strain is minimized, there can be differences in the surface properties of the material which can affect device performance and also impurities from the substrate can diffuse into the device itself. Atomic Force Microscopy reveals the surface properties and Secondary Ion Mass Spectroscopy can detect minute concentrations of impurities. Both techniques are employed in this study.

2. Detailed X-Ray Characterization of GaN and AlGaN Materials

GaN-based materials have attracted much attention for optoelectronic device applications where there is a need to operate in the blue-green regime.[1] However, the high threading dislocation density in the III-Nitrides is an issue that encumbers their further development as optoelectronic devices in the ultraviolet.[2] The threading dislocation (TD) density is normally determined using plan view transmission electron microscopy (TEM), however this technique is destructive and typically requires a few days before the data can be obtained.[3] X-Ray Diffraction (XRD) has been used to obtain functionally equivalent data from some average measurements of crystal microstructure. Since XRD is a non-destructive and rapid characterization technique it is the most common technique used to optimize crystalline quality growth parameters. GaN is different from other compound semiconductor materials because it is formed with large columnar areas of crystalline material that are misaligned to each other, i.e. a mosaic structure.[4] Thus an estimate of size of those domains, the average misorientation between them and dislocation density is important in optimizing material growth. High-resolution XRD reciprocal space mapping (RSM) is normally utilized for detailed characterization of such crystalline structures. However, a much quicker and simpler method to obtain similar information utilizes the Williamson-Hall (WH) plot.

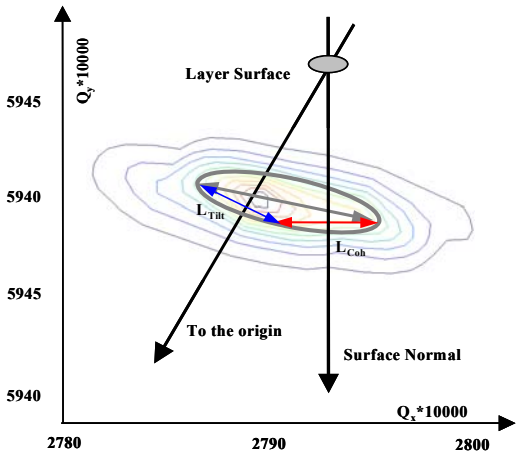

Figure 1: $(1\bar{1}0\ 4)$ RSM of GaN #1. L_{coh} is the length of the FWHM component parallel to surface, and L_{ll} is the reciprocal L_{coh}. α_{tilt} is derived by the length of component perpendicular to origin direction. In addition, α_{tilt} can be obtained from (0004) RSM.

In this study of GaN and AlGaN, RSM and WH plot techniques were used to characterize the columnar structures and to evaluate the threading dislocation densities of thin layers grown by MOCVD. These two methods are compared for consistency and to investigate the effect of Al composition in AlGaN alloys on dislocation density.

2.1 Theory

Reciprocal space mapping (RSM) of a reflection plane can be plotted by recording equivalent intensities from a series of Ω scans each having a different detector position with respect to the 2Θ direction (Ω-2Θ scans). Since the linewidths of these scans for RSM are broadened by size (coherence lengths) and angular misorientation (tilt and twist angles) of the columnar structure, the RSM is used to obtain information about the columnar structure. As illustrated in Figure 1, the lateral coherence length (L_{ll}) is the reciprocal of the component of the FWHM parallel to the surface (L_{coh}) in the RSM of an asymmetric reflection.[5] On the other hand, from the RSM of a symmetric (000*l)* reflection plane, the tilt angle (α_{tilt}) is the vertical component of the FWHM ellipse. Lastly, from the RSM of reflection planes in the a-axis direction, the vertical component of the FWHM ellipse is twist angle (α_{twist}). [6,7,8]

Another technique for obtaining L_{ll} and α_{tilt} is through the use of Williamson-Hall (WH) plots. For this technique, the broadening of the Ω scan (rocking curve) of the symmetric reflections is affected only by the tilt and the coherence length parallel to the reflection surface. WH plots make it possible to distinguish these two broadening mechanisms.[9] When $\beta_\omega(\sin\theta)/\lambda$ is plotted against $(\sin\theta)/\lambda$ for each reflection and a straight line is fitted, the y-intersect (Y_o) of the fitted line is used to estimate the lateral coherence length, L_{ll} (= 0.9 / 2Y_o) [2,10,11,12], where β_ω, θ, and λ are the integral width of the measured profile, the Bragg reflection angle, and the X-Ray wavelength, respectively. In addition, the slope of the fitted line corresponds to the tilt angle, α_{tilt}. Moreover, α_{twist} is found from a Φ-scan on asymmetric reflections. In this work, it is assumed that the columnar structure does not abruptly change over the reflection planes, so the information from a specific reflection by using RSM method can be compared to the mean values obtained from the WH method.

Using the data obtained from RSM or WH method, different dislocation densities can be determined. This is done through the use of Burgers vectors and elucidated in the calculations given below. GaN layers have three main types of threading dislocation (TD) densities; screw

dislocation along the c-axis [0001], edge dislocation in the a-axis [$11\bar{2}0$] and mixed screw and edge dislocations. In this work the mixed dislocations are ignored because they should have much lower densities than pure screw or edge dislocation. Screw and edge dislocation densities are distinguished by Burgers vectors b_c = [0001] and b_a = ⅓ [$11\bar{2}0$] respectively. The tilt angle is used to determine the screw dislocation density, $N_{screw,}$ with the Burgers vector $|b_c|$ by [2,11]

$$N_{screw} = \alpha_{tilt}^2 / (4.35 \, |b_c|^2) \quad (2)$$

The same is done with twist angle to determine the edge dislocation density, N_{edge}, with the Burgers vector $|b_a|$, the majority of the dislocations occur at the small angle grain boundaries, [2]

$$N_{edge} = \alpha_{twist} / (2.1 \, |b_a| \, L_{ll}) \quad (3)$$

This dislocation density is a function of the Burgers vector that is directly expressed by the lattice constant of the films. For dislocation densities of $Al_xGa_{1-x}N$ layers, therefore it is necessary to find their lattice constants. The lattice constant of an alloy can be derived using Vegard's law ($a(Al_{1-x}Ga_xN) = xa(AlN) + (1-x)a(GaN)$ which is a relation between the composition and the lattice constant. [13]

2.3 Experimental Details

In this work, all samples were grown by Metalorganic Chemical Vapor Deposition (MOCVD) in an EMCORE D180 short jar system on (0001) on sapphire. TMGa, TMAl and NH_3 were used as the source precursors for Ga, Al, and N, respectively. A 30nm low-temp (540 °C at 300 Torr) GaN nucleation layer was used for undoped GaN samples #1, #2, and #3 which are 2.2, 1.9 and 2.2 um thick, respectively. The GaN epilayers were grown at 1050 °C with a V/III ratio of 4000 and a growth rate of ~2μm/h. A 25 nm low-temperature (590 °C at 300 Torr) AlN nucleation layer was used for AlGaN epilayers. Sample #4, $Al_{0.15}Ga_{0.85}N$, was grown at 900 °C on a 2 μm GaN buffer layer with a V/III ratio of 33000 and a growth rate of ~0.15 μm/h. Alloy samples #5 ($Al_{0.4}Ga_{0.6}N$) and #6 ($Al_{0.62}Ga_{0.38}N$) and the AlN sample were grown at 1080 °C on low-temperature AlN nucleation layers with a V/III ratio of 4000 and a growth rate of 0.5, 0.3 and 0.2 μm/h, respectively.

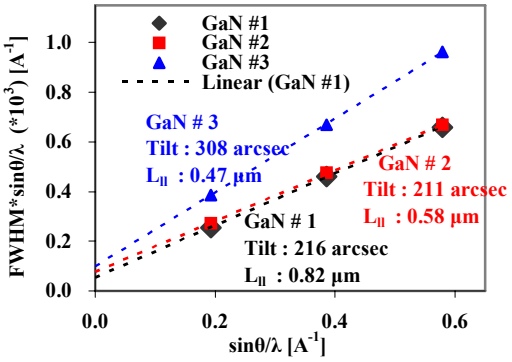

Figure 2: Williamson-Hall Plots for undoped GaN samples #1, #2, and #3.

In-situ reflectometry was used to monitor the growth rate and the surface morphology.

XRD measurements were performed with a Philips X'pert MRD triple-axis diffractometer equipped with a four bounce Ge (022) monochromator and a Cu sealed anode. An Ω scan and a 2Θ- Ω scan on the symmetric (0002), (0004), and (0006) reflection planes as well as RSMs on (0004), $(1\bar{1}\ 0\ 4)$, and $(1\bar{2}1\ 1)$ reflection planes were performed. In addition, Φ-scans were completed on each sample.

2.4 Results

Undoped GaN

A reciprocal space mapping (RSM) of GaN #1 is shown in Figure 1, from which lateral coherence length is determined as the reciprocal of L_{coh}. In addition, the α_{tilt} and α_{twist} are given by (0004) and $(1\bar{2}1\ 1)$ RSMs (not shown here), respectively. Furthermore, $L_{||}$, α_{tilt}, and α_{twist} are determined in the same manner for GaN #2 and #3.

WH plots have also been used to extract values for $L_{||}$ and α_{tilt} for these samples in Figure 2. Values for α_{twist} were obtained directly from Φ-scans on asymmetric reflections.

The data for GaN obtained by both these techniques is summarized in Table 1. The mean N_{screw}

	Method	GaN #1	GaN #2	GaN #3
L_{ll} [um]	WH plot RSM	0.82 0.33	0.58 0.25	0.48 0.28
Tilt [aresec]	WH plot RSM	216 274	211 266	308 335
Twist [arcsec]	Φ scan RSM	835 792	662 655	792 702
N_{scew} [cm^{-2}]	WH plot RSM	9.4E+07 1.5E+08	9.0E+07 1.4E+08	1.9E+08 2.3E+08
N_{edge} [cm^{-2}]	WH plot RSM	7.4E+08 1.7E+09	8.3E+08 1.9E+09	1.2E+09 1.8E+09

Table 1: Summary of the mosaic structure factors of GaN samples #1, #2, and #3 by various methods

with the Burgers vector ($|b_c|$=5.185 Å) and N_{edge} with the Burgers vector ($|b_a|$=3.189 Å) obtained using a WH plot have been compared with these obtained using RSM. The α_{tilt} values by WH are larger than these by RSM methods. This may be explained by annihilation of the defects with respect to the growth direction (i.e. c-axis) during the growth process.[14, 15] Since the tilt angle along the c-axis is relaxed during growth, the average α_{tilt} by WH is smaller than a transition α_{tilt}

value by RSM. While the mean L_{ll} by WH is smaller than a transition L_{ll} value by RSM, since L_{ll}, a component length with respect to parallel to surface, is smaller as α_{tilt} is larger. These differences lead to dissimilarity between two methods for N_{screw} and N_{edge} due to relaxation of defect during growth. The WH plot provides the mean size and angular distribution of the columnar structure from a combination of the (0002), (0004), and (0006) reflections, while RSM provides a specific value from a specific reflection. Therefore, the WH plot may be expected to provide a more reliable estimate of the average values for the columnar structure of GaN, even though RSM measurements will provide more accurate information. It should be noted that the values obtained for N_{screw} and N_{edge} are less accurate than those typically measured by TEM and this is being investigated.[3] However, both the WH plot and RSM still allow a relative measure of material quality.

$Al_xGa_{1-x}N$/Nucleation layer on Al_2O_3

Based on the previous two methods for GaN samples, AlGaN epitaxial layers have also been investigated. Figure3 exhibits AlGaN #4 RSMs of asymmetric and symmetric reflection planes which provide L_{ll} and α_{tilt}. While α_{twist} is given by $(1\bar{2}1\,1)$ RSMs (not shown here). AlGaN #5 and #6 were also performed in the same way. These RSMs have two peaks corresponding to the GaN and the AlGaN layers, respectively. The GaN peak is stronger than the diffraction corresponding to the AlGaN layer in Fig, 3 (a). A thicker layer (2 um GaN > 0.2 um $Al_{0.15}Ga_{0.85}N$) leads to a stronger XRD intensity as well as sharper peak.

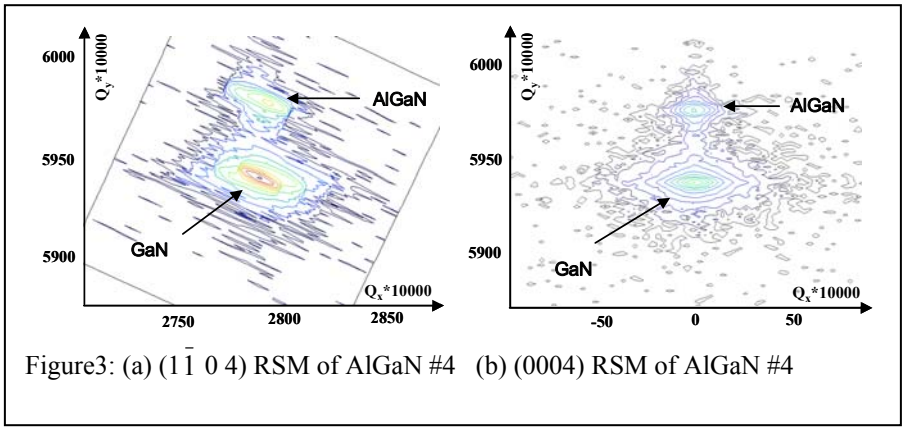

Figure3: (a) $(1\bar{1}\,0\,4)$ RSM of AlGaN #4 (b) (0004) RSM of AlGaN #4

Figure 4 depicts the WH plots which provide $L_{||}$ and α_{tilt}. $Al_{0.15}Ga_{0.85}N$ layer of AlGaN #4 on

GaN nucleation layer seems to have values similar to those of GaN samples. Whereas, AlGaN #5 and #6 grown on AlN nucleation layers have quite different values. The difference is probably caused by relaxation of the underlying layer. This relaxation associated with layer thickness can influence the columnar structure of the AlGaN layer and also cause cracking in this layer.[16] In addition, the AlGaN samples have larger tilt angles and smaller coherence lengths as the Al composition increases.

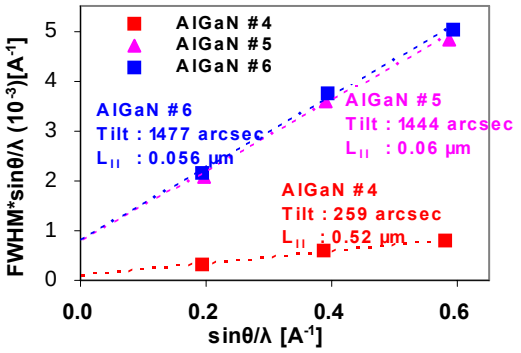

Figure 4: Williamson-Hall plots for $Al_xGa_{1-x}N$ layers of AlGaN #4, #5, and #6. Different nucleation layer cause this quite difference between AlGAN #4 and AlGaN #5 (or #6)

Dislocation density is a function of Burgers vector that is directly indicated by lattice constant of the layer. 2Θ scans on the (0004) reflection are measured to evaluate the lattice constants of AlGaN #4, #5, and #6. Thus, from the measurement data, the Burgers vectors of the c-axis and the a-axis for $Al_xGa_{1-x}N$ alloys can be easily determined as $|b_c|$ =5.153 and $|b_a|$=3.177 Å, $|b_c|$=5.101 and $|b_a|$=3.158 Å, and $|b_c|$=5.055 and $|b_a|$=3.141 Å for AlGaN samples #4, #5, and #6, respectively.

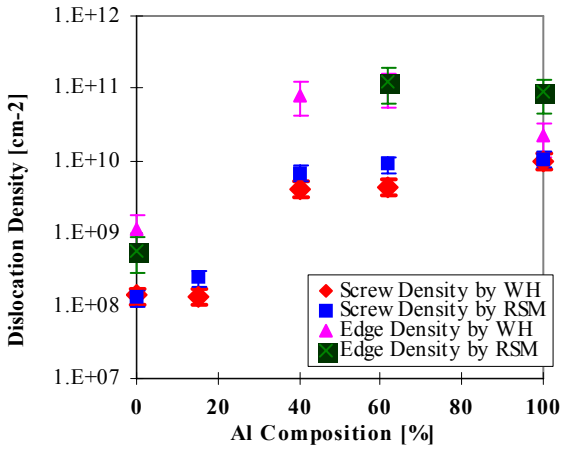

Figure 5: Screw and edge densities with Al composition for AlGaN #4, #5, and #6

The variation of the screw and edge densities with Al composition measured by WH and RSM is shown in Figure 5. It is apparent that AlGaN (< 40% Al) grown on a GaN nucleation layer shows lower densities of screw and edge dislocations than those grown on AlN nucleation layers (> 40% Al). Moreover, the screw dislocation density shows a systematic increase with Al composition in the $Al_xGa_{1-x}N$ layers (> 40% Al). The growth mechanism could change with increasing Al; however, further measurements are needed before this conclusion can be reached.

Table 2 shows the mean geometric size of the columnar structures as well as the dislocation

densities for the epitaxial AlGaN layers. Some values are not reported due to the weak XRD intensity and, as a consequence, these measurements have large error bars. Moreover, the values

	Methods	AlGaN #4 GaN layer	AlGaN #5 $Al_{0.15}Ga_{0.85}N$ layer	AlGaN #6 $Al_{0.4}Ga_{0.6}N$ layer	AlGaN #6 $Al_{0.62}Ga_{0.38}N$ layer	AlN AlN layer
L_{ll} [um]	WH plot	0.51	0.52	0.06	0.056	0.27
	RSM	0.62	0.46	0.05	0.054	0.06
Tilt [arcsec]	WH plot	265	259	1444	1477	2140
	RSM	256	349	1857	2120	2232
Twist[arcsec]	Φ scan	831	NA	6804	8496	8028
	RSM	493	NA	NA	9457	7380
N_{screw} [cm^{-2}]	WH plot	1.4E+08	1.4E+08	4.3E+09	4.4E+09	1.0E+10
	RSM	1.3E+08	2.5E+08	7.2E+09	9.5E+09	1.1E+10
N_{edge}[cm^{-2}]	WH plot	1.2E+09	NA	8.3E+10	1.1E+11	2.2E+10
	RSM	5.8E+08	NA	NA	1.3E+11	9.0E+10

Table 2: Summary of the mosaic structure factors of AlGaN samples #4, #5, and #6 by various methods

obtained for L_{ll}, α_{tilt} and α_{twist} by WH and RSM for are in closer agreement than GaN; i.e. specific values aren't much varied since defects are less relaxed due to the smaller thickness and different type of nucleation layers.

3. HEMT Structures on SiC and Si wafers

High Electron Mobility Transistors were fabricated using AlGaN on silicon and silicon carbide substrates. Since these substrates have different crystal structures and lattice parameters, there is always some inherent strain present when AlGaN is grown on them. Furthermore there are questions about contaminants from the substrate diffusing into the transistor's active layers which will be investigated with SIMS.

3.1 High Resolution X-ray Diffraction

AlGaN HEMT on Si

Three measurements, corresponding to the wafer flat edge, center and round edge were taken for each wafer. In order to accurately determine the strain in such materials, X-ray diffraction rocking curves or reciprocal space maps are required, as noted in the section above [17]. The rocking curve method assumes that the lattice parameters of the substrate provide a good reference, which is indeed the case here. The symmetric peak of the GaN (002) plane (the symmetric plane) was measured using the Omega-2Theta (ω-2θ) scan and is depicted in Figure 6.

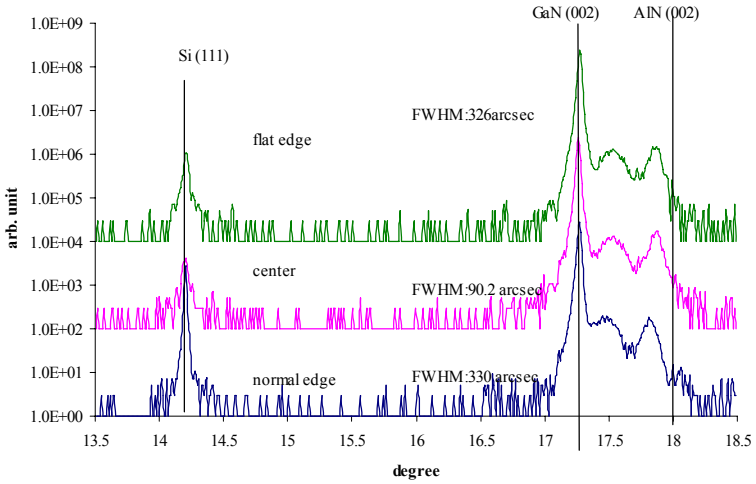

Figure 6: Omega-2Theta scan for the AlGaN HEMT structures grown on Si. The three points were all measured on the same wafer.

The substrate peaks, Si (111), are shown as a reference of the GaN peaks. The AlN/AlGaN buffer layer was grown between the GaN film and the Si substrate. The AlN peaks are small, suggesting that the AlGaN on the GaN is relaxed, and shifted by approximately 0.2°. This shift may indicate that the AlN layers are under strain in the superlattice structure. The peaks between AlN and GaN are the AlGaN buffer layer. The relative omega positions of the GaN and the substrate show that the GaN layer grown on Si is almost relaxed. It is apparent that $Al_xGa_{1-x}N$ (< 40% Al) grown on the GaN nucleation layer shows lower densities of screw and edge

dislocations than films grown on AlN nucleation layers. Moreover, the screw density in $Al_xGa_{1-x}N$ layers (> 40% Al) shows a systematic increase with Al composition. The growth mechanism could be expected to change with increasing Al; however, further measurements are needed before this conclusion can be verified.

	Measured c	Relaxed c	Strain (%)
Flat	5.18542036	5.185508	-1.69E-03
Center	5.18634841	5.185508	1.62E-02
Round	5.18557162	5.185508	1.23E-03

Table 3: Rough strain calculation from the X-ray measurement for HEMT on Si (111) surface.

Defining the strain as the ratio of the difference in the lattice constants when relaxed and when strained to the relaxed constant

Strain $\equiv \{(C_{measured}-C_{relaxed})/ C_{relaxed}\}$ x 100%, where c is the out-plane lattice constant

the strain at the three places on the wafer is shown in Table 3. The strain is <0.002% for these AlGaN layers grown on Si(111).

AlGaN HEMTs on SiC

As expected from polarization observations the SiC contains many low angle grain boundaries, and is more strained than the growth on Si wafer. The omega-2theta (ω-2θ) scan along the GaN 002 direction is shown in Figure 7. The accompanying strains in the films are calculated and presented in Table 4, below. The AlN peak is

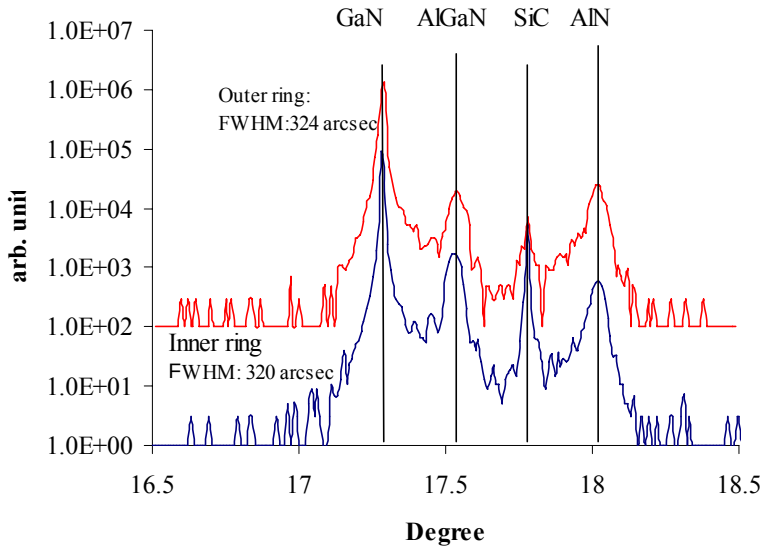

Figure 7: Omega-2Theta scan for the AlGaN HEMT structures grown on SiC.

properly on 18° indicating that the AlN in this HEMT structure is relaxed; however, the strain in the AlGaN layers, in contrast, is over 1000X larger than the strain measured in Si. This result indicates that any growths undertaken on SiC must be carefully checked for strain problems.

	Measured c	Relaxed c	Strain (%)
Outer	5.0944	5.1855	-1.758
Inner	5.0961	5.1855	-1.724

Table 4: Rough strain calculation from the X-ray measurement for the HEMT structure on the SiC wafer..

Within-run variability was investigated by measuring the XRD on a SiC wafer without any accompanying structure. Both the symmetric (002) and asymmetric peaks (106) were measured on the three points of one SiC wafer and are shown below in Figure 8. The film quality is not uniform with very different FWHM depending on the location on the wafer. Strains and defects exist inside the substrate itself and increased towards the edge. These defects, already present in the substrate, could explain the large strain observed in the AlGaN HEMT structures.

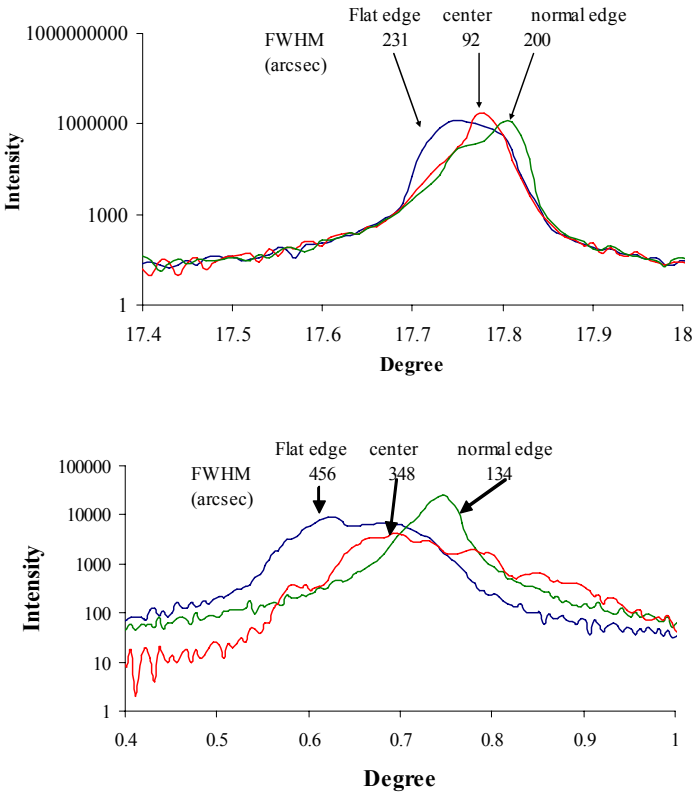

Figure 8: HR XRD scans of the SiC substrate. Upper scan is of the (002) peak in three locations on the wafer. The lower scan is of the (106) peak. Both peaks show the large intra-run variability over this one wafer.

3.2 Atomic Force Microscopy

AlGaN HEMT on Si

Atomic Force micrographs were taken of the samples in question with a Digital Nanoscope scanning probe microscope employed in contact mode. The scanned area is a 10μm by 10μm square. The films grown on Si, shown in Figure 9, have by far the roughest surfaces measured. To be certain of the cause measurements on the surface of plain silicon wafers would need to be measured.

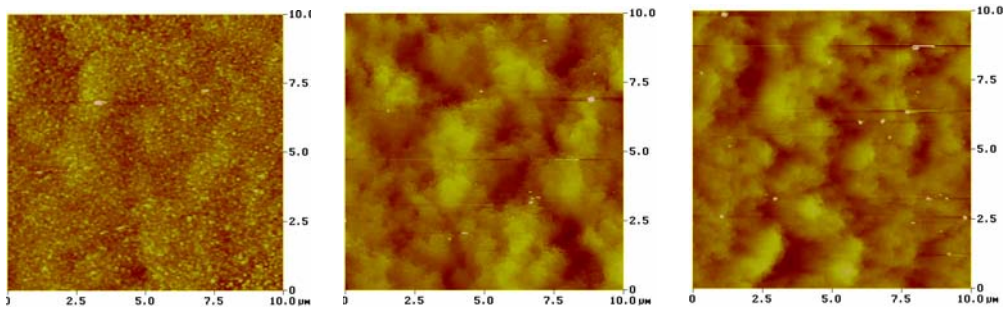

Figure 9: AFM depictions of the AlGaN layers grown on silicon. Each depiction is a 10 micron by 10 micron square. The left picture is taken near the wafer flat, the center at the wafer's center, and the right picture near the wafer round.

AlGaN HEMT on SiC

Under an optical microscope, scratches of the second film (outer ring) can be observed all over the surface of the HEMT on SiC. Despite these blemishes, the overall mean surface roughness of the HEMTs on SiC was an order of magnitude lower than that measured on the HEMTs on Si. The AFM result is shown in Figure 10 below. To see whether the native SiC surface was smoother than the Si surface, a SiC substrate was also measured, and shown in Figure 11.

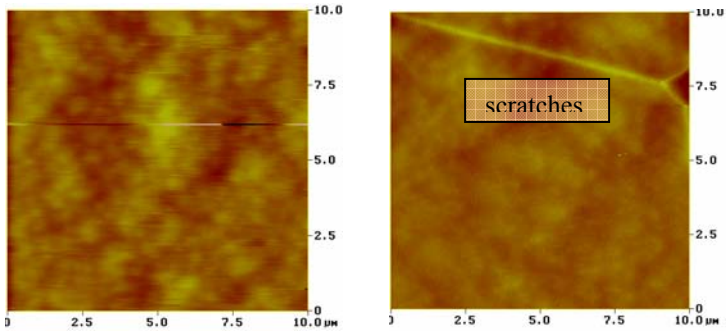

Figure 10: AFM depictions of AlGaN layers grown on silicon carbide. Each figure represents a scanned area of 10 microns square. The left figure refers to the inner ring; the right figure to the outer ring.

SiC substrate

Three points were measured on the SiC substrate. It seems that the central portion of the wafer is even smoother than the center part. However, inspection of the wafer under an optical microscope revealed the presence of rough surfaces between the center and the round edge. These areas were not measured using AFM; however they do contribute to the impression of a lack of wafer uniformity.

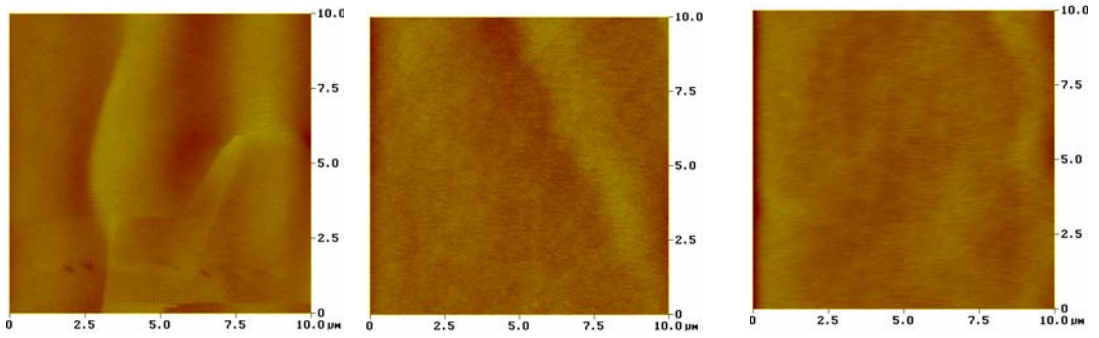

Figure 11: AFM depictions of the SiC substrate surface. Each picture shows a square 10 microns on each side. The left figure is for the wafer flat, the center figure for the center of the wafer, and the right figure for the wafer round edge.

Comparison of XRD and AFM data on HEMT structures

Wafers of silicon and silicon carbide were employed as substrates for the fabrication of AlGaN/GaN HEMTs. The issues of strain can predominate in HEMT manufacture and the tools of AFM and high resolution XRD were employed to examine this issue with similar HEMT structures grown on both types of substrates. The HEMT structures on silicon carbide substrates had significantly lower surface roughness than the structures on plain silicon (0.715nm vs 2.61nm) (see Table 5). However, the silicon

	Wafer part	rms Roughnesss (nm)
SiC wafer	round	0.165
	center	0.179
	flat	0.605
	average	0.316
HEMT on SiC	inner	0.609
	outer	0.812
	average	0.715
HEMT on Si	round	2.35
	center	2.41
	flat	3.09
	average	2.61

Table 5: Comparison of mean surface roughness for HEMTs on silicon carbide and silicon substrates.

carbide-based HEMTs had significantly higher strain (–1.74% vs < 0.002%) than the Si-based ones (see Tables 3 and 4). We hypothesize that strain relief might cause the roughening on the Si surface while relieving some of the layers of their strain.

3.3 Secondary Ion Mass Spectroscopy

A SIMS depth profile was performed on an AlGaN HEMT structure grown on a Si substrate. A cesium beam was used to sputter the sample; however, because no standard was available at that time, the actual concentrations could not be determined. Furthermore, in any superlattice structure, it is difficult to determine the absolute concentrations due to the effects of the matrix on the ion yield. Thus the count rate given in Figure 12 is only relative to other points in the wafer with the same matrix. From this figure, very little silicon diffusion is observed inside the film from the underlying silicon wafer. It is apparent that the superlattice helps to decrease the Si diffusion. To elucidate this mechanism, whether the superlattice acts as a getter, or whether it is simply a more effective barrier to Si diffusion, remains to be determined. Both carbon and oxygen, the most common impurities present in AlGaN and GaN thin films are also present mostly in the top surface AlGaN layer and in the superlattice structure on top of the Si substrate. This could indicate several origins of the contamination: possibly the Al-source is contaminated with O or C, AlGaN acts as a getter, or diffusion from the underlying substrate and from the surface. Despite apparently very large O and C signals, the actual abundances of oxygen and carbon are much smaller than those of Si and Al. The discrepancy occurs because of the much higher ion yields for C and O in GaN when using the Cs beam.

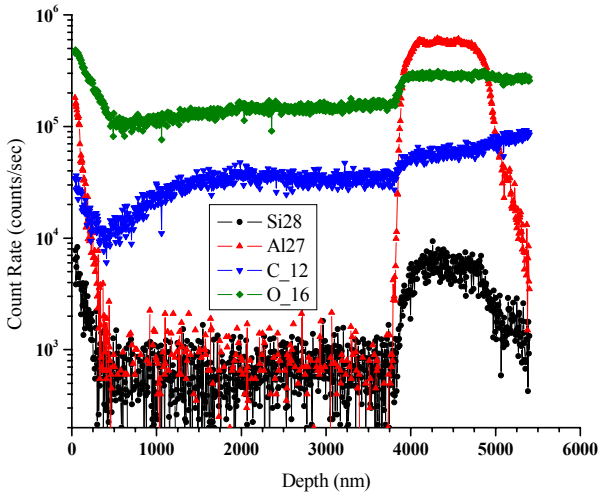

Figure 12: SIMS depth profile of HEMT structure using a Cs ion beam on silicon showing the presence of residual oxygen and carbon as well as the presence of Si doping and Al alloys. The surface artifacts well known in SIMS have already been edited out of this graph.

4. Conclusion

In this work, we have studied both AlGaN films using X-ray diffraction and also studied HEMT structures on two types of substrates. The first part of this work investigated the typical mosaic structures of GaN on sapphire with the Williamson-Hall and Reciprocal Space Mappin methods by XRD measurements. The effects of not only the columnar structure's size and angular uniformity, but also the Al composition in the epitaxial AlGaN layers on threading dislocation (TD) density have been investigated. In addition, the TD is influenced by the type and thickness of the nucleation layer. The second portion of this study looked at the growth of AlGaN-based HEMT structures grown atop silicon and silicon carbide substrates. Growth of AlGaN on top of these lattice-mismatched substrates results in strain observed in the XRD data, although, curiously, the SiC substrates showed one thousand times greater strain than measured in the Si substrates. The AFM data support the view that growth, even with a superlattice, on top of silicon yielded a much rougher surface than growth on silicon carbide. The SIMS data show some silicon in the superlattice and near the surface, regions which also show increased oxygen and carbon contamination, although the mechanism is unclear.

References

[1] C. Kim, and J. Je, Mat.Res. Soc. Symp.595, W3.52.1 (2000)

[2] T. Metzger, R. Hopler, E. Born, and O. Ambacher, Phil. Mag. A, 77, 1013 (1998)

[3] F. Ponce Microstructure of Epitaxial III-V Nitride Thin Films, 141 1997

[4] T. Cheng, L. Jenkins, S. Hooper, and C. Foxon , Appl. Phys. Lett. **66**, 1509 (1995).

[5] P.F. Fewster, X-Ray Scattering from semiconductors 263 (2000)

[6] P.F. Fewster, X-Ray and Neutron Dynamical Diffraction: Theory and Applications, NATO ASI Series B: Physics 357 287 (1996)

[7] P.R. Fewster, N. L. Andrew, and C.T. Foxon, J. Cryst. Growth 230, 404, (2001)

[8] D.K. Bowen, High Resolution X-ray Diffractometry and Topography, 149 (2001)

[9] G.K. Williamson and W.H. Hall, Acta. Metall. 1, 22 (1953)

[10] T. Metzger, R. Hopler, E. Born, and S. Christiansen, Phys. Stat. Sol. A 162, 529 (1997)

[11] H.Wang, J. Zhang, C. Chen, Q. Fareed, and J. Yang, Appl. Phys. Lett., 81, 605 (2002)

[12] H. Heinke, V. Kirchner, S. Einfeldt, and D. Hommel, Phys. Stat. Sol. A 172, 391 (1999)

[13] P.Bhattacharya, Semiconductor Optoelectronic Devices, 5 (1997)

[14] S. Molina, A. Sanchez, F. Pacheco, and R. Garcia, Appl. Phys. Lett. 74, 3362 (1999)

[15] L. Kirste, D. Ebling, C. Haug, and K. Tillmann, Mater. Sci. Eng., B 82 9 (2001)

[16] B. Bennett, Appl. Phys. Lett. 73, 3736 (1998)

[17] P.F. Fewster, X-Ray Scattering from Semiconductors, Oxford; Inst. Phys. Conf. Ser. No. **164,** 197 (1999).

[18] H. Kang, N. Spencer, D. Nicol, Z.C. Feng, and I. Ferguson*, unpublished paper.